Nanotechnology, Science and Applications

Dovepress

open access to scientific and medical research

Open Access Full Text Article

ORIGINAL RESEARCH

# Green Nanotechnology Through Papain Nanoparticles: Preclinical in vitro and in vivo Evaluation of Imaging Triple-Negative Breast Tumors

Aryel H Ferreira[1–3,*], Fábio LN Marques[4], Caroline C Real[5], Velaphi C Thipe[6,*], Lucas F Freitas[1,2], Caroline SA Lima[1,2], Larissa Estessi de Souza[4], Mara S Junqueira[7], Daniele de Paula Faria[4], Gustavo HC Varca[1], Ademar B Lugão[1], Kattesh V Katti[6,8,*]

[1]Nuclear and Energy Research Institute, IPEN-CNEN/SP, Sao Paulo, 05508-000, Brazil; [2]MackGraphe - Mackenzie Institute for Research in Graphene and Nanotechnologies, Mackenzie Presbyterian University, Sao Paulo, 01302-907, Brazil; [3]Mackenzie Evangelical College of Paraná - Mackenzie Presbyterian University, Curitiba-PR, 80730-000, Brazil; [4]Laboratory of Nuclear Medicine (LIM-43), Departamento de Radiologia e Oncologia, Faculdade de Medicina FMUSP, Universidade de Sao Paulo, Sao Paulo, 05403-911, Brazil; [5]Aarhus University, Department of Nuclear Medicine & PET-Centre, Aarhus, Denmark; [6]Department of Radiology, Institute of Green Nanotechnology, University of Missouri, Columbia, MO, 65212, USA; [7]Center for Translational Research in Oncology, Cancer Institute of the State of Sao Paulo, Faculty of Medicine, University of Sao Paulo, Sao Paulo, Brazil; [8]Department of Biotechnology & Food Technology, University of Johannesburg, Johannesburg, South Africa

*These authors contributed equally to this work

Correspondence: Kattesh V Katti, Department of Radiology, Institute of Green Nanotechnology, University of Missouri, Columbia, MO, 65212, USA, Email kattik@health.missouri.edu; Aryel H Ferreira, MackGraphe-Mackenzie Institute for Research in Graphene and Nanotechnologies, Mackenzie Presbyterian University, Consolação Street 930, São Paulo, 01302-907, Brazil, Email aryel.ferreira@mackenzie.br



**Background:** Recent advancements in nanomedicine and nanotechnology have expanded the scope of multifunctional nanostructures, offering innovative solutions for targeted drug delivery and diagnostic agents in oncology and nuclear medicine. Nanoparticles, particularly those derived from natural sources, hold immense potential in overcoming biological barriers to enhance therapeutic efficacy and diagnostic accuracy. Papain, a natural plant protease derived from *Carica papaya*, emerges as a promising candidate for green nanotechnology-based applications due to its diverse medicinal properties, including anticancer properties.

**Purpose:** This study presents a novel approach in nanomedicine and oncology, exploring the potential of green nanotechnology by developing and evaluating technetium-99m radiolabeled papain nanoparticles ($^{99m}$Tc-P-NPs) for imaging breast tumors. The study aimed to investigate the efficacy and specificity of these nanoparticles in breast cancer models through preclinical in vitro and in vivo assessments.

**Methods:** Papain nanoparticles (P-NPs) were synthesized using a radiation-driven method and underwent thorough characterization, including size, surface morphology, surface charge, and cytotoxicity assessment. Subsequently, P-NPs were radiolabeled with technetium-99m ($^{99m}$Tc), and in vitro and in vivo studies were conducted to evaluate cellular uptake at tumor sites, along with biodistribution, SPECT/CT imaging, autoradiography, and immunohistochemistry assays, using breast cancer models.

**Results:** The synthesized P-NPs exhibited a size mean diameter of 9.3 ± 1.9 nm and a spherical shape. The in vitro cytotoxic activity of native papain and P-NPs showed low cytotoxicity in HUVEC, MDA-MB231, and 4T1 cells. The achieved radiochemical yield was 94.2 ± 3.1% that were sufficiently stable (≥90%) for 6 h. The tumor uptake achieved in the 4T1 model was 2.49 ± 0.32% IA/g at 2 h and 1.51 ± 0.20% IA/g at 6 h. In the spontaneous breast cancer model, 1.19 ± 0.20% IA/g at 2 h and 0.86 ± 0.31% IA/g at 6 h. SPECT/CT imaging has shown substantial tumor uptake of the new nanoradiopharmaceutical and clear tumor visualization. $^{99m}$Tc-P-NPs exhibited a high affinity to tumoral cells confirmed by ex vivo autoradiography and immunohistochemistry assays.

**Conclusion:** The findings underscore the potential of green nanotechnology-driven papain nanoparticles as promising agents for molecular imaging of breast and other tumors through SPECT/CT imaging. The results represent a substantial step forward in the application of papain nanoparticles as carriers of diagnostic and therapeutic radionuclides to deliver diagnostic/therapeutic payloads site-specifically to tumor sites for the development of a new generation of nanoradiopharmaceuticals.

Received: 7 June 2024
Accepted: 19 September 2024
Published: 25 September 2024

**Graphical Abstract**

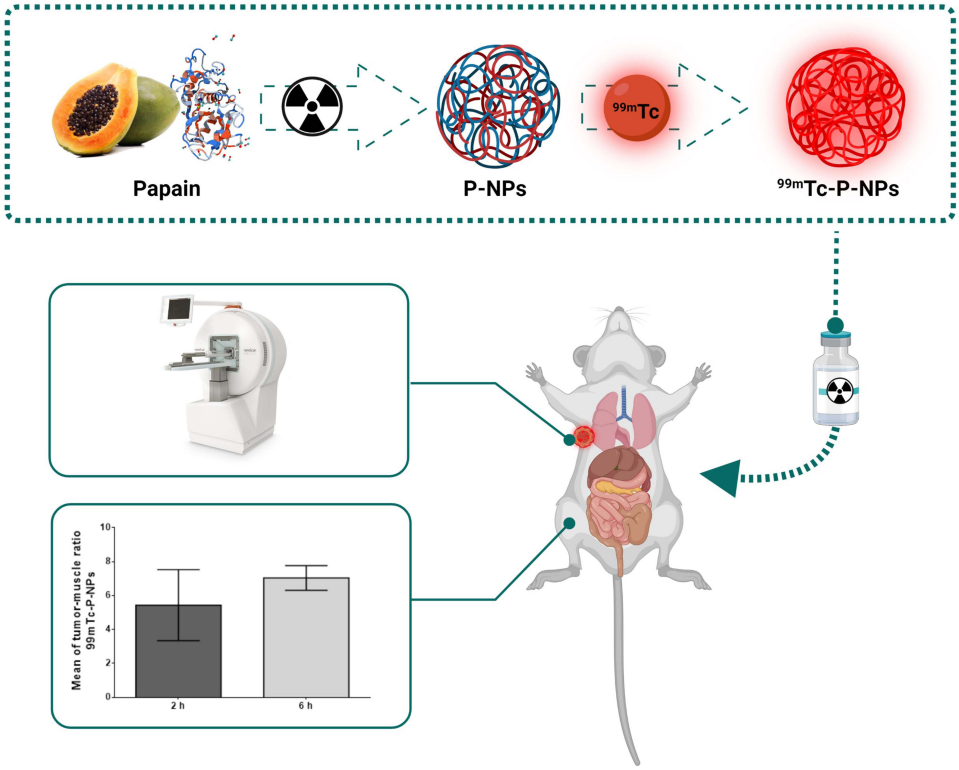


**Keywords:** papain nanoparticle, protein nanoparticle, enzymatic nanoparticle, imaging probe, nanoradiopharmaceuticals

## Introduction

In recent years, there has been a significant focus on discovering new biocompatible nanomaterials sourced from natural resources. These materials have the potential to inhibit cancer, reduce the likelihood of cancer occurrence, and facilitate the precise delivery of therapeutic and diagnostic agents to specific sites.[1–3] Green nanotechnology, which emphasizes environmentally friendly methods and materials, plays a crucial role in this field. Additionally, integrating herbal medicines, known for their natural therapeutic properties, into nanotechnology enhances their efficacy.[4] This is particularly significant in the case of triple-negative breast cancer (TNBC), an aggressive form of breast cancer characterized by rapid progression and high metastasis rates, resulting in a poor prognosis and limited targeted therapeutic options.[5,6]

Plant proteases are attractive platforms for designing protein nanoparticles due to their advantageous physicochemical properties, including thermal stability with high enzymatic activity, solubility, and simplicity of plant extraction at low cost.[7,8] Papain, an enzyme in the protease category, is extracted from the latex of *Carica papaya*, commonly referred to as papaya. With a molecular weight of 23.5 kDa, this enzyme consists of 212 amino acids organized into two domains. Cysteine, histidine, and aspartic acid characterize its active site.[9] Its therapeutic properties, including anticancer, antibacterial, and antioxidant capabilities, make it an excellent candidate for medical applications.[10,11]

Papain is involved in various biological activities, including proteolysis, cell dissociation, and wound cleanser formulations to remove necrotic tissue and promote recovery in skin treatments, attributed to the reduction activity of thiol groups.[12,13] Numerous studies conducted by various groups have demonstrated that papain has anticancer effects.[14–22] Papain's effectiveness in modulating cell signaling pathways in the immune system, apoptosis, and cancer

development has been shown in vitro using several cancer cell lines.[23] In vivo studies in animal models have demonstrated its efficacy in inhibiting primary and metastatic tumor development (melanoma and Lewis lung carcinoma).[18,24]

Additionally, animal models treated with proteases survive substantially longer than those untreated.[18] Clinical trials in breast, colorectal, and plasmacytoma cancer patients demonstrated that adjunctive systemic enzyme therapy (containing papain) reduced tumors as well as reduced therapy-induced adverse effects.[14,25] While several in vitro and in vivo investigations have been conducted to elucidate its broad spectrum of pharmacological effects, little is known regarding its pharmacokinetic properties and toxicological profile.

The development of papain nanoparticle-based imaging probes for nuclear imaging allows for pinpointing disease locations, tracking changes in pathology and gaining insights in molecular aspects linked to payload delivery. Gaining a thorough insight into biodistribution and pharmacokinetics behavior in vivo is valuable in guiding therapeutic and diagnostic interventions involving nanoscale drug delivery systems of papain nanoparticle-based imaging probes. The promising pharmacological properties of papain prompted us to develop an enzymatic protein-based nanoparticle system to enhance tumor uptake and bioavailability and capitalize on papain's potential efficacy as a nanocarrier to deliver contrast agents and diagnostic radionuclides successfully.

The tumor extracellular matrix (ECM) represents a significant barrier to the delivery of drugs and radionuclides, particularly in non-vascularized and anoxic tumor regions. This ECM, composed of proteoglycans, hyaluronic acid, collagen, and other structural proteins, limits delivery effectiveness.[26] To address this challenge, we have developed papain nanoparticles that actively degrade the ECM, enhancing the delivery and efficacy of diagnostic agents and molecules within the tumor. This approach aims to improve the uniform distribution of agents throughout the tumor parenchyma, potentially overcoming the limitations of current therapeutic and diagnostic strategies.

Notably, no published studies have examined the use of papain nanoparticles, especially those obtained using radiation, with anticancer potency to deliver radionuclides to tumor sites for diagnosis purposes.

In continuation of our long-standing efforts in the development of nano-sized radiopharmaceuticals,[27–38] we herein, describe innovative synthetic pathways to produce papain nanoparticles (P-NPs) by gamma irradiation, their radiolabeling with technetium-99m ($^{99m}$Tc), and evaluation of in vitro parameters. Toward our overall objective of developing SPECT imaging probes for the accurate diagnosis of breast tumors, we also describe, herein as a proof of concept, in vivo imaging biodistribution investigations of technetium-99m ($^{99m}$Tc) radiolabeled papain nanoparticle ($^{99m}$Tc-P-NPs) using breast tumor bearing mice.

# Materials and Methods

## Preparation of Papain Nanoparticles

Papain nanoparticles were synthesized using the radiation-induce method following Varca et al and Fazolin et al[9,39] Papain nanoparticles were synthesized in an ice bath using 10 mg.mL$^{-1}$ of papain dissolved in 50 mm phosphate buffer (pH 7.4) containing 20% (v/v) ethanol. At a dose rate of 5 kGy.h$^{-1}$, samples were subjected to γ-irradiation in the ice to a dose of 10 kGy using $^{60}$Co as a radioactive source in a multipurpose irradiator (IPEN/CNEN-Brazil).

## Nanoparticles Characterization

### Particle Size Distribution and Zeta Potential Measurements

The analysis of particle size distribution, encompassing mean diameter and polydispersity index, was conducted employing the Zetasizer Nano ZS (Malvern Instruments, Worcestershire, UK). A 1 mg.mL$^{-1}$ suspension of P-NPs was prepared in MilliQ water. Subsequently, a 10 µL aliquot was diluted to 1 mL of MilliQ water. The average diameter was computed based on three determinations for each sample. In the same equipment, appropriate diluted samples were used to measure the zeta potential at 25°C. The values presented denote the mean ± standard deviation derived from a minimum of three distinct batches of nanoparticles.

### Field Emission Scanning Electron Microscopy (FEG-SEM)

The surface morphology of P-NPs was examined through field emission scanning electron microscopy (FEG-SEM) using a JSM 7800F (JEOL, Japan). Before imaging, the samples underwent sputter-coating with gold (6 nm thickness) using a Balzers SCD 050 apparatus at a current intensity of 22 mA for 60s. The image capture was conducted with an accelerating voltage maintained at 0.5 kV.

## Papain Nanoparticles in vitro Cytotoxicity

The potential cytotoxic effects of native papain and P-NPs were assessed against MDA-MB-231 (human triple-negative breast cancer cell line-ATCC), 4T1 (an animal model for stage IV human breast cancer-ATCC), and HUVEC (Human Umbilical Vein Endothelial Cells – Sigma Aldrich) using the MTT assay. MDA-MB-231, 4T1, and HUVEC cell lines were cultured in DMEM or RPMI-1640 medium. The cells were seeded at a density of $1_{\times}10^4$ cells per well in 96-well plates and maintained at 37°C in a humidified atmosphere with 5% $CO_2$. After 48 h, the respective media were replaced with 200 µL of fresh media containing varying concentrations of native papain and P-NPs (5–100 $\mu g.mL^{-1}$ for 48 h). Following the incubation period, media containing free native papain and P-NPs were aspirated, and 200 µL of MTT solution (1 $mg.mL^{-1}$) was added to each well, with further incubation for 4 h at 37°C in the dark. Upon removal of the culture medium, 150 µL of DMSO was added to each well to dissolve the intracellular formazan crystals, and absorbance was measured at 550 nm using a microplate reader (VersaMax, Molecular Devices).

Cell viability was calculated using the formula:

$$\text{Cell viability } (\%) = \frac{\text{Abs test cells}}{\text{Abs control cells}} \text{x } 100$$

Here, *Abs test cells* represent the formazan amount for cells treated with native papain or P-NPs, and *Abs control cells* express the intra-cellular formazan in non-treated cells.

## $^{99m}$Tc Radiolabeling of Papain Nanoparticles

P-NPs were radiolabeled with technetium-99m ($^{99m}$Tc) by the direct-labeling method using tin chloride dihydrate as a reducing agent. Briefly, 500 µL of aqueous sodium pertechnetate ($Na^{99m}TcO_4^-$; 555–740 MBq) was added to 200 µL of P-NPs suspension (equivalent to 2 mg P-NPs) followed by the addition of 10 µL (22 mM) of freshly prepared tin chloride dihydrate (nitrogen-purged 0.1N HCl solution) and incubated for 30 min at 45°C. After cooling at room temperature, the samples were filtered using 0.2 µm PVDF filters (13 mm).

The radiolabeling efficiency was determined by paper chromatography using 1.0 × 8.0 cm Whatman 1 paper as the stationary phase with two mobile phases: 1) acetone and 2) pyridine: acetic acid: water (3:5:1.5) as per the previously reported procedure (Figure S1).[40,41]

## In vitro Evaluation of $^{99m}$Tc-Labeled P-NPs

### In vitro Stability Studies of $^{99m}$Tc-Labeled P-NPs

The in vitro stability of $^{99m}$Tc-P-NPs was evaluated using a method previously outlined.[42] In summary, radiolabeled nanoparticles (0.1 mL-74 MBq) were individually introduced into 0.9 mL of (a) serum and (b) histidine solution ($1_x10^{-2}$ M). Then, these mixtures were incubated at 37°C for 24 h. Samples were withdrawn at different time points (0, 1, 3, 6, and 24 h) and subjected to analysis through paper chromatography (as previously described) to detect any potential dissociation of the radiolabeled formulation.

### In vitro Cell-Binding and Internalization of $^{99m}$Tc-Labeled P-NPs

The cell binding and internalization of $^{99m}$Tc-P-NPs in MDA-MB-231 and 4T1 cell lines were investigated following a method previously outlined with some adjustments.[43] Briefly, cells were cultured in triplicate in six-well plates ($1_x10^5$ cells/well) with DMEM or RPMI medium at 37°C for 24h. Subsequently, approximately 37 kBq of $^{99m}$Tc-P-NPs were introduced into the medium, and the cells were incubated at 37°C in 5% $CO_2$ for various time intervals (15, 30, 60, 90,

and 120 min). After each specified time, the medium was removed to halt cellular internalization, and the cells were washed with ice-cold phosphate-buffered saline (pH 7.2).

The gamma counter (Hydex, Finland) was employed to measure radioactivity in both cell pellets (total bound) and the supernatant (unbound). Cell surface-bound radioligand was removed by washing the cells with ice-cold acidic buffer (0.05 $mol.L^{-1}$ glycine solution, pH adjusted to 2.8 with 1N HCl) for 5 min. The remaining cell-associated radioactivity, resistant to this procedure, was considered internalized radioactivity. Finally, trypsin treatment at 37°C for 5 min was applied to detach cells from the plates. The supernatant was collected, and the radioactivity was measured. The percentage of internalized radioactivity was computed following previously described methods. Each experiment underwent three repetitions, and the results were presented as the mean ± standard deviation.

## In vivo Evaluation of $^{99m}$Tc-Labeled P-NPs

The Ethics Committee in Animal Use of the Faculty of Medicine of the University of São Paulo (FMUSP 128/16) approved all animal studies and experimental protocols. All experiments were conducted according to the guidelines set by the National Council for Animal Experimentation Control (CONCEA-Brazil).

## Biodistribution in Healthy Balb/c Mice, 4T1 Tumor-Bearing Mice, and Spontaneous Breast Cancer Mice (MMTV-PyMT)

Biodistribution studies were performed in healthy Balb/C (n = 3) and spontaneous breast cancer mice (n=3, MMTV-PyMT). For the 4T1 tumor-bearing model, freshly collected 4T1 cells ($2_x10^7$ cells) suspended in saline were injected into mice via intraductal injection (through the mammary gland closest to the thigh of the right hind paw). After two weeks, a palpable tumor (volume $1 \pm 0.1$ $cm^3$) was developed, and the animals were used for biodistribution studies. $^{99m}$Tc-P-NPs (0.1 mL, 37–74 MBq) were administrated by intravenous (IV) injection through the tail vein of all the well-hydrated animals. At 2 and 6 h post-injection, the animals (n = 3) were euthanized, and the blood sample was collected by cardiac puncture, as well as organs and tissues. All mice were acquired from the Faculty of Medicine of the University of São Paulo.

All the samples were collected in pre-weighed scintillation vials, and the radioactive counts were measured using a gamma counter (Hidex, Turku, Finland). Organ uptake was expressed as a percentage of the injected activity per gram of tissue (% IA/g) or organ.

### SPECT/CT Image

SPECT/CT images were acquired in a dedicated small animal scanner (Triumph™- Gamma Medica-Ideas, Northridge, CA, USA). All procedures were performed with the animals under anesthesia (2–3% isoflurane in 100% oxygen). $^{99m}$Tc-P-NPs, 37 MBq in 0.1 mL, was administrated intravenously into the tail vein (n=3/time). After 2 and 6 h $^{99m}$Tc-P-NPs post-injection, animals were positioned with the tumor region in the center of the SPECT scanner field. A dual-head camera with 1.0 mm five-pinhole collimators and a CZT detector system was used. The SPECT image was acquired for 30 minutes (32 projections of 60s each per detector). Heating pads maintained the animals' body temperature and breath rate was monitored.

After the scans, the animals were allowed to recover in their home cages. Images were reconstructed using the Ordered subset expectation maximization OSEM 3D algorithm. Before or after SPECT acquisition, computed tomography (CT) images, 45 kVp, and 360 μA were obtained during 1 min (256 projections, 1.3x magnification). CT images were reconstructed with FBP (filtered back projection) algorithm with a 512 × 512 matrix and 0.17 × 0.17 mm pixel. SPECT/CT fused images were analyzed using PMOD® software. The volume of interest (VOI) was manually drawn for each animal in the breast tumor. The data is presented as the ratio between tumor and muscle uptake.

## Ex vivo Autoradiography

After SPECT/CT acquisition, the animals were deeply anesthetized with 5% isoflurane in 100% oxygen and euthanized by heart extirpation. The breast tumor was dissected and frozen in the tissue freezing medium (OCT, Tissue-Tek). Slices of the tumor were prepared at cryostat (30 μm) and collected on histological slides. After that, slides with tumor tissue

were exposed to a multi-sensitive phosphor storage screen for 24 h. The exposed phosphor screens were scanned in a Typhoon FLA 9500 biomolecular image (GE Healthcare). The distribution profile of $^{99m}$Tc-P-NPs binding in the tumor slice was observed at ImageJ (NIH, USA).

### Immunohistochemistry

The same tumor used for ex vivo autoradiography was employed to prepare histological material for immunohistochemistry. However, the tumor tissue sections were thinner (10 µm). As a result, the data constitutes a series of adjacent slices for autoradiography and immunoassay. Histological slides with tumor slices were stored at −20°C until the immunohistochemistry procedures.

For immunostaining, we used an anti-papain antibody (goat polyclonal, Novus Biologicals, NBP2-44059) and, as the secondary antibody, a biotinylated donkey anti-goat IgG (705–065-147, Jackson Immuno Research Laboratories Inc). In brief, to remove endogenous peroxidase, slides containing the tumor sections were incubated at 0.3% hydrogen peroxide solution for 10 min and then washed with PBS (3 times for 10 min). Thus, tumor tissue sections were incubated overnight at 22°C with 1:200 dilution of the primary antibody solution containing 5% normal goat serum in 0.3% Triton X-100 in PBS. Then, sections were incubated for 2 h with a 1:200 diluted secondary antibody solution. Afterward, the sections were processed for 2 h using the ABC Elite kit at 1:100 (Vector Labs, Burlingame, CA, USA) and labeled 0.05% diaminobenzidine tetrahydrochloride (DAB, D5637-25G, Sigma). Sections were incubated for 5 min in DAB solution. After that, 5 drops of 0.3% hydrogen peroxide in PBS were added until the slices became brown, when they were rewashed with PBS. Histological slides were treated with 0.05% osmium tetroxide in water, dehydrated, and cleared with Xylol, and the coverslip was mounted using Permount mounting medium (Fisher, Pittsburg, PA, USA).

Digital images of stained sections were acquired using a Nikon DMX1200 digital camera to illustrate the papain distribution in the tumor.

## Results

### Synthesis and Characterization of Papain Nanoparticle

Radiation-synthesized P-NPs exhibited a size profile in the mean diameter 9.3 ± 1.9 nm range as determined through dynamic light scattering (DLS). They exhibited a zeta potential of −11.1 ± 5.5 mV—thus rendering optimal in vitro stability against agglomeration. The surface characteristics of P-NPs were examined using field emission scanning electron microscopy (FEG-SEM). SEM images revealed the spherical nature of P-NPs, and the particle distribution histogram corroborated particle sizes of 13.7 ± 6.5 nm, consistent with the mean observed through DLS analyses (Figure 1A–C).

### In vitro Cytotoxicity of Papain Nanoparticles

In vitro cytotoxic activity of native papain and P-NPs was determined by MTT assays in two invasive ductal/breast carcinoma cell lines: MDA-MB-231 (ATCC), and 4T1 (ATCC). We have also used HUVEC cells (Sigma-Aldrich) to assess papain nanoparticles toxicity. Generally, incubation periods were chosen at 48 h to avoid incorrect results that may

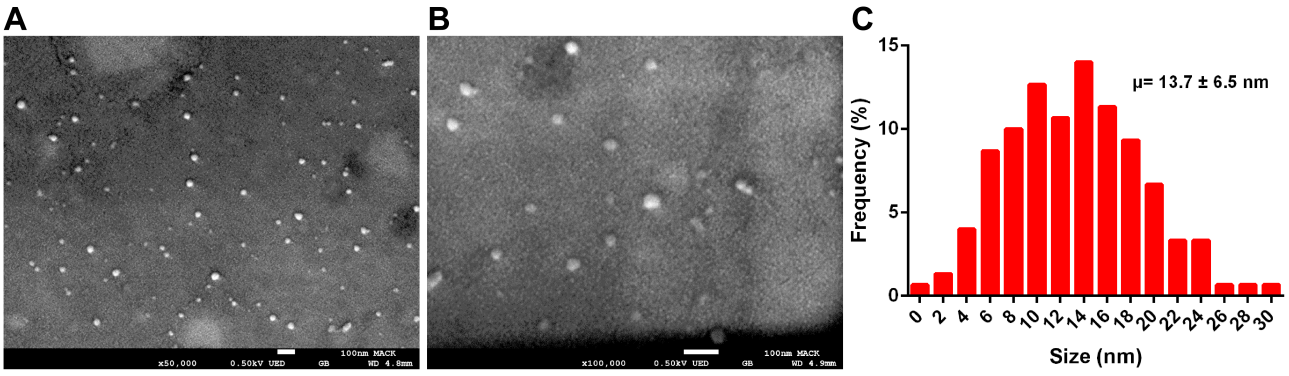


**Figure 1** Characteristics of P-NPs. (**A** and **B**) SEM image and (**C**) Particle size distribution histogram obtained from SEM images.

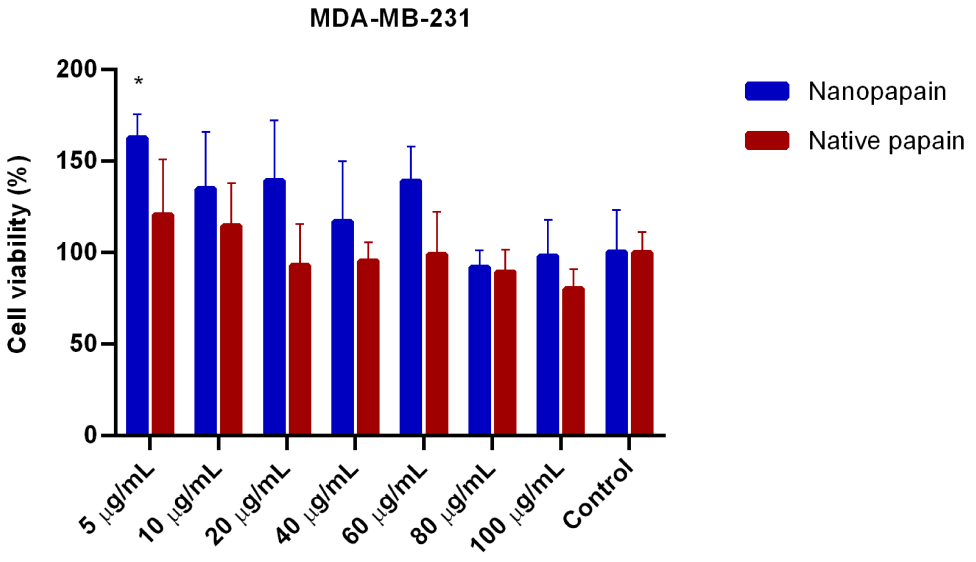


**Figure 2** Cell viability of MDA-MB-231 breast cancer cells incubated with different papain concentrations, either in nanoparticle or native forms. *Statistically significant difference with both controls ($p<0.001$).

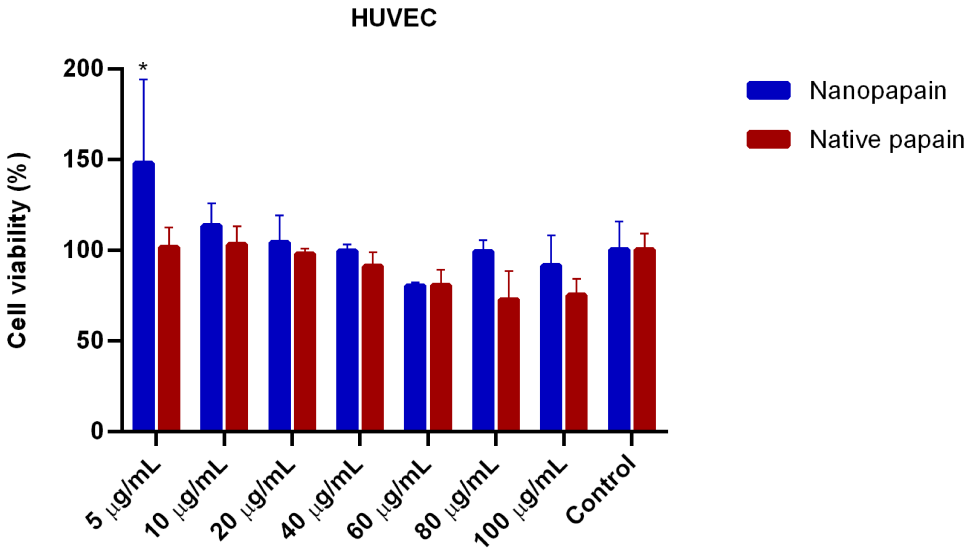


**Figure 3** Cell viability of HUVEC healthy human endothelial cells incubated with different papain concentrations, either in nanoparticle or native forms. *Statistically significant difference with both controls ($p<0.001$).

arise due to the trypsin-like effects of papain (papain can detach cells; however, after 48 hours its activity over the cell culture is decreased to the point that the detachment effect is negligible, and the cells are fixed on the plate again). All cell lines presented similar results, and low papain cytotoxicity was observed (none of the conditions led to <75% viability, except for the highest concentration of native papain to 4T1 cells). All the samples' means were not statistically different from the control cells in MDA-MB-231 and HUVEC lines. In contrast, native papain presented mild toxicity in 4T1 cells exposed to the highest concentrations of the enzyme (Figures 2–4).

## $^{99m}$Tc Labeling, Quality Control, and Stability Studies

Radiolabeling parameters, including the quantity of nanoparticle suspension, reducing agent, and incubation time were carefully standardized to attain a consistently high level of reproducible purity. The assessment of purity was conducted using paper chromatography. P-NPs were successfully labeled with $^{99m}$Tc, showing a radiochemical yield of 94.2 ± 3.1%

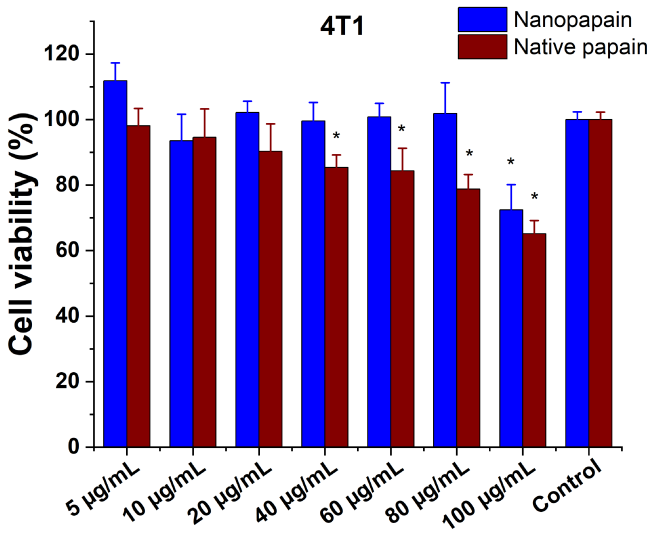


**Figure 4** Cell viability of 4T1 mice metastatic breast cancer cells incubated with different papain concentrations, either in nanoparticle or native forms. *Statistically significant difference with both controls ($p<0.05$).

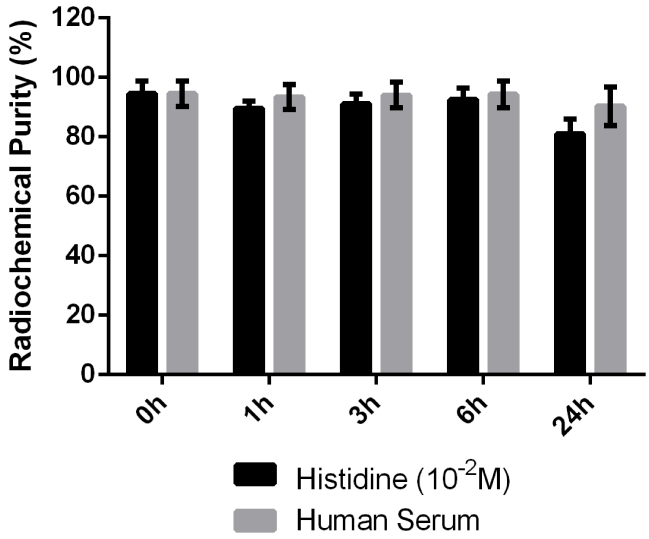


**Figure 5** Stability study parameters of $^{99m}$Tc labeled P-NPs in histidine and human serum.

after $^{99m}TcO_2$ removal using 0.22 µm PDVF filter membrane. Radiochemical impurity ($^{99m}TcO_4^-$) was quantified as 5.8% using paper chromatography (Figure S2).

$^{99m}$Tc labeled P-NPs ($^{99m}$Tc-P-NPs) were sufficiently stable (≥90%) for 6 h when incubated with histidine solution ($10^{-2}$ M) and freshly collected human serum at 37°C (Figure 5). After 24 h of incubation, an average of 18.9 and 9.7% degradation occurred in histidine solution and serum, respectively, demonstrating that the radiolabeled nanoparticle is highly stable in vitro and sufficiently stable for transchelation. According to these stability studies (Figure 5), the radiolabeled nanoparticle may exhibit sufficient in vivo stability during biological studies.

## In vitro Cell Binding and Biological Evaluation

The $^{99m}$Tc-P-NPs were examined for their tumor-targeting properties in vitro using the human MDA-MB-231 (ATCC) and murine 4T1 breast cancer cell lines (ATCC). The cellular uptake and internalization behavior of $^{99m}$Tc-P-NPs as a function of time is presented in Figure 6. Following 15 min incubation with $^{99m}$Tc-P-NPs, around 0.88 ± 0.17% of the total activity was bound to 4T1 cells, increasing to 1.46 ± 0.15% after 2 h incubation. After 15 min incubation, about 20.82 ± 4.73% of

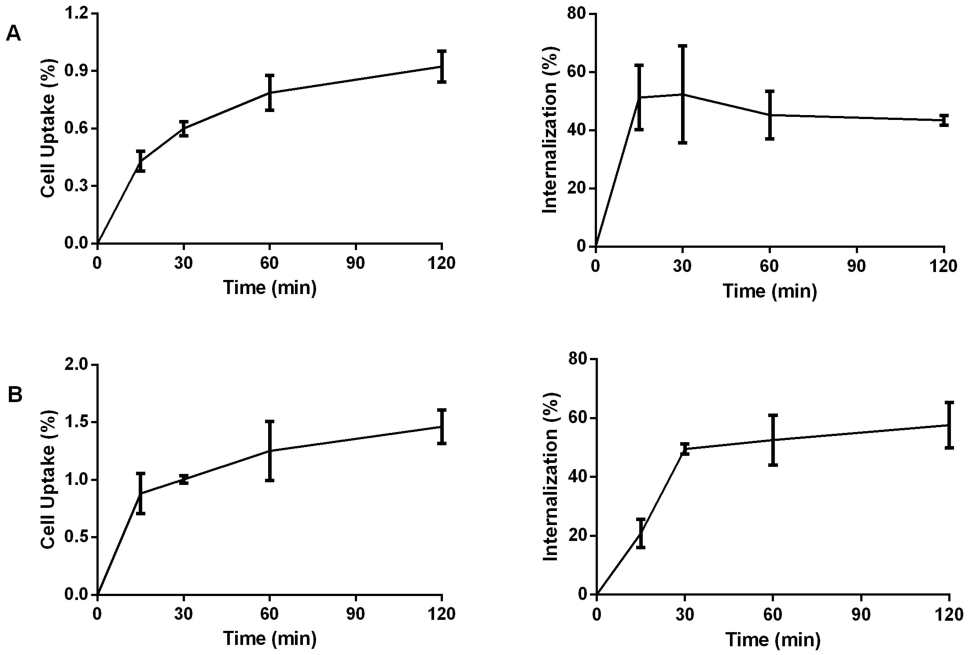


**Figure 6** In vitro cell binding and internalization of $^{99m}$Tc labeled P-NPs in (**A**) MDA-MB231 cells and (**B**) 4T1 cells at different time intervals.

the cell-associated activity was internalized, gradually rising to around 52.62 ± 7.68% after 2 h. For MDA-MB231 cells, about 0.43 ± 0.05% of the total activity of $^{99m}$Tc-P-NPs was bound after 15 min, and 51.26 ± 11.09% was internalized after 2 h, the value reached a high of 0.92 ± 0.08% with total internalization around 43.42 ± 1.66%.

As the in vitro behavior was similar between MDA-MB231 and 4T1 cells, the murine model was used for tumor growth. This model is frequently used testing experimental drugs in triple-negative breast cancers. This model presents aggressive solid tumors in mice with similarities to triple-negative breast tumors in humans.[44–46] Likewise, MMTV-PyMT mice were chosen because they can develop spontaneous mammary tumors that closely resemble the progression and morphology of human breast cancers.[47]

Figures 7 and 8 summarize the biodistribution studies of $^{99m}$Tc-P-NPs at 2 and 6 h post intravenous injection in healthy mice, 4T1 xenograft mice model, and spontaneous breast cancer model MMTV-PyMT, respectively. The radiotracer showed moderate blood clearance in healthy mice, 3.30 ± 0.48% IA/g after 2 h. However, 4T1 and MMTV-

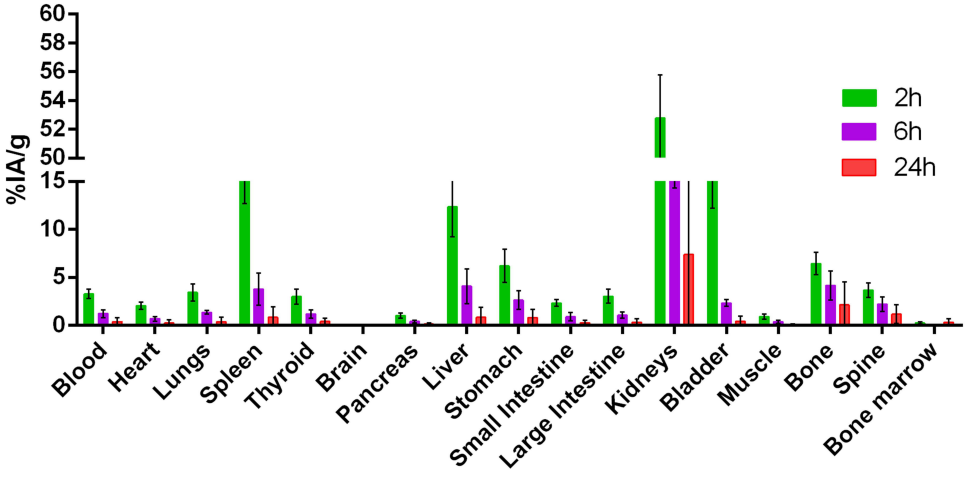


**Figure 7** Biodistribution studies of $^{99m}$Tc labeled P-NPs in balb/c healthy mice at 2 and 6 h post-injection (%IA/g).

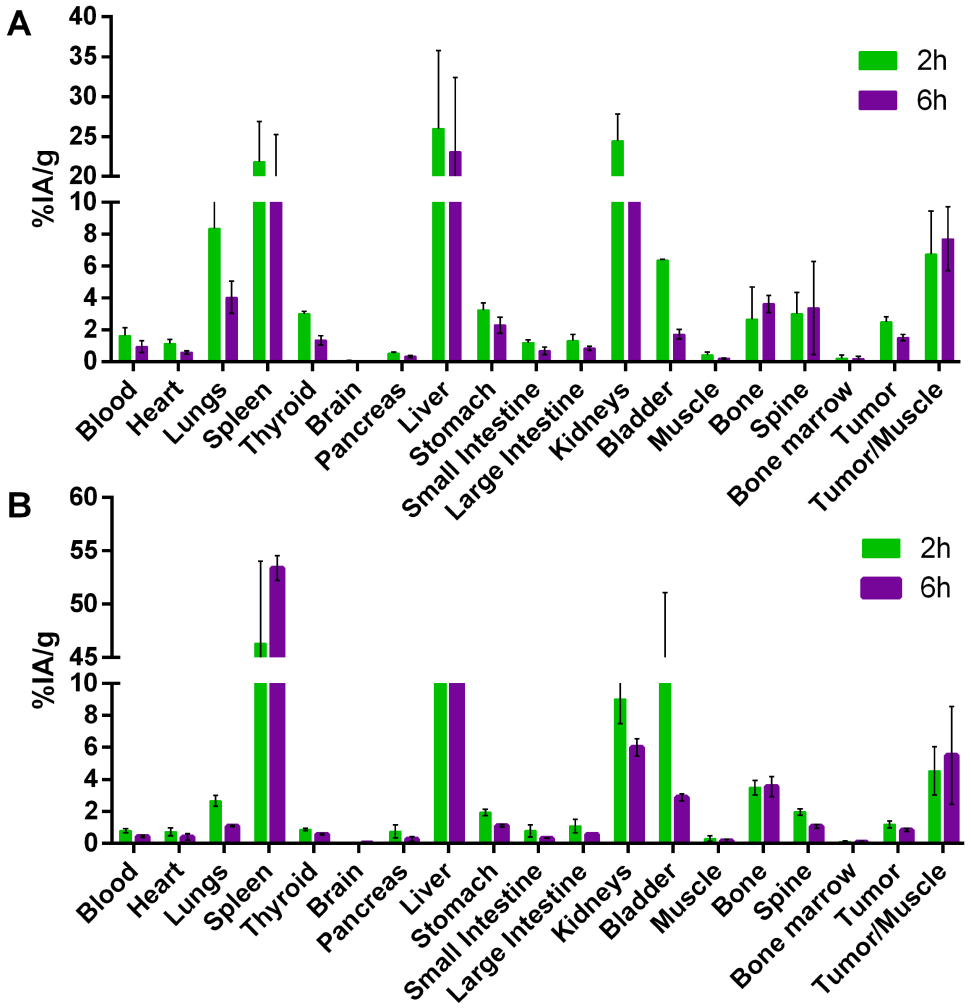


**Figure 8** Biodistribution studies of $^{99m}$Tc labeled P-NPs in (**A**) 4T1 tumor-bearing mice and (**B**) spontaneous breast cancer mice (MMTV-PyMT) at 2 and 6 h post-injection (%IA/g).

PyMT models showed rapid clearance with 1.63 ± 0.50% IA/g and 0.80 ± 0.13% IA/g, respectively, followed by subsequent reduction at 6 h due to biodistribution and accumulation in reticuloendothelial system (RES) organs.

Furthermore, the uptake of $^{99m}$Tc-P-NPs in the spleen and liver was expected considering that nanoparticles may be removed from the bloodstream through opsonization followed by phagocytosis. The pancreas, small intestine, and large intestine demonstrated a minimal uptake of $^{99m}$Tc-P-NPs for all models, confirming the hydrophilicity of the nanoparticles. Radioactivity uptake for most tissues was lower in tumor-bearing mice and MMTV-PyMT mice than in healthy animals, particularly the kidney. In contrast to healthy animals, $^{99m}$Tc-P-NPs in RES organs uptake of animals with cancer almost tripled for the 4T1 model and tenfold for MMTV-PyMT at 6 h, and the difference was found to be two-fold between cancer models under the same conditions.

These findings indicated that $^{99m}$Tc-P-NPs were excreted primarily through the renal-urinary system, with secondary clearance occurring via the hepatic system. Tumor accumulation of the nanoparticle diminished over time. The highest tumor uptake was achieved in the 4T1 model when compared to spontaneous breast cancer mice: 2.49 ± 0.32% IA/g vs 1.19 ± 0.20% IA/g at 2 h ($p < 0.05$) and 1.51 ± 0.20% IA/g vs 0.86 ± 0.31% IA/g at 6 h ($p < 0.05$). The tumor-to-blood ratio was not high but remained constant until 6 h. Nonetheless, tumor-to-muscle ratios were significantly higher in both animal models over the investigated time. The 4T1 model achieved the best ratios, especially for tumor/muscle ratio outcomes (Figure 9).

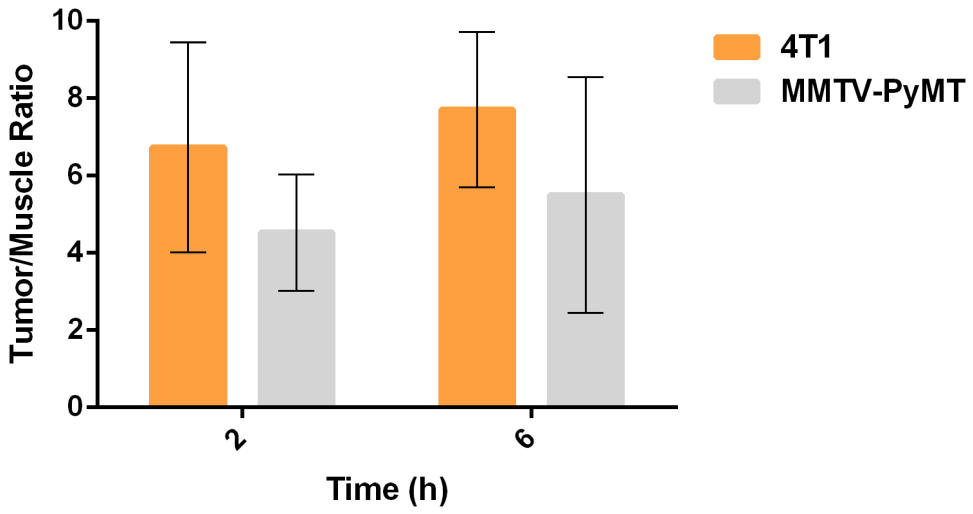


**Figure 9** Ex vivo means of tumor–muscle ratio uptake in 4T1 tumor-bearing Balb/C mice ($n$ = 3) evaluated by SPECT at 2 and 6 h post intravenous (IV) injection of $^{99m}$Tc-P-NPs.

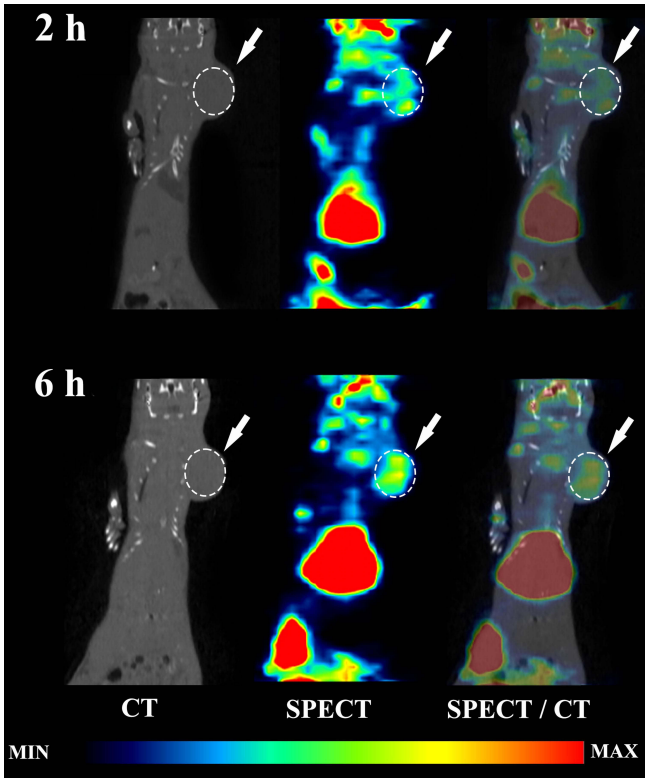


**Figure 10** In vivo biodistribution of $^{99m}$Tc-P-P-NPs in 4T1 tumor-bearing Balb/C mice. SPECT/CT images of $^{99m}$Tc-P-NPs injection at 2 and 6 h post-injection in mice following the intravenous (IV) injection.

Our SPECT/CT imaging investigations in breast tumor bearing animal models have shown substantial tumor uptake of the new nanoradiopharmaceutical, $^{99m}$Tc-P-NPs, as shown in vivo (Figure 10) and ex vivo (Figure 8). The rapid blood clearance, increased tumor–muscle ratio, and tomographic images all aided in delineating the region of interest (ROI) index of the tumor (Figure 12). The mean uptake in the 4T1 model was 42% higher at 6 h (6.46 ± 7.04) after IV injection when compared to 2 h (3.74 ± 5.43) (Figure 9). The affinity of $^{99m}$Tc-P-NPs to tumoral cells was also confirmed by autoradiography and immunohistochemistry assays (Figure 11). Note that there is a similarity location of high uptake of $^{99m}$Tc-P-NPs

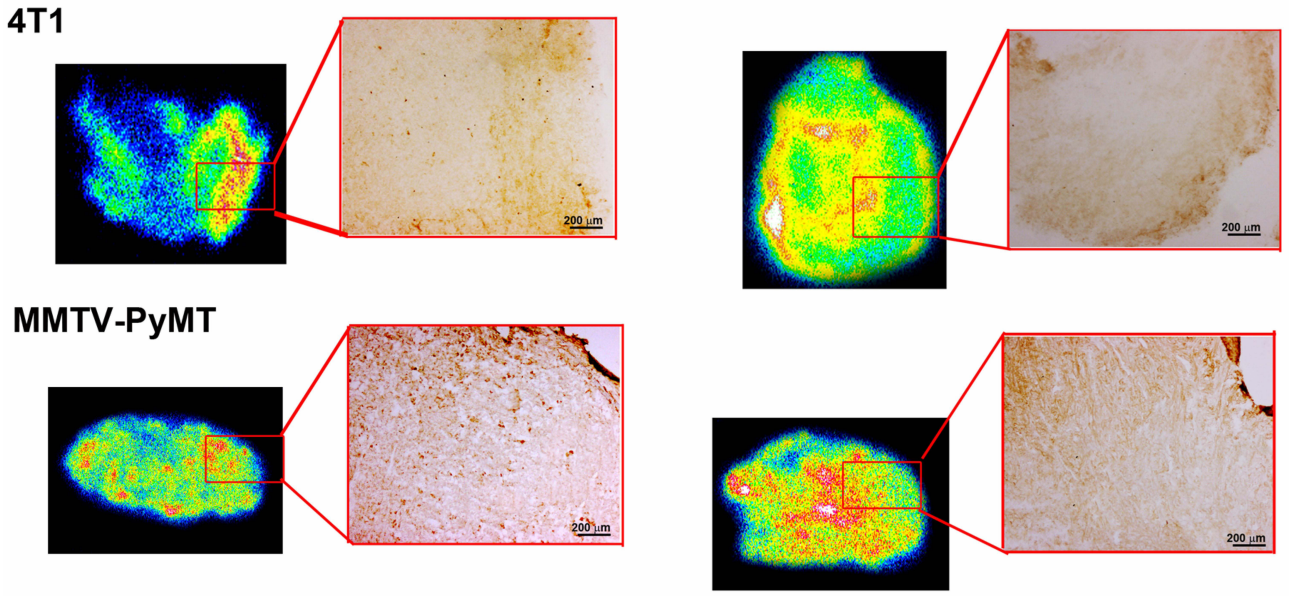


**Figure 11** Autoradiography of $^{99m}$Tc-P-NPs and immunohistochemistry for papain in 4T1 tumor-bearing Balb/C mice and MMTV-PyMT. Experiments were performed immediately after SPECT acquisition at 2 and 6 h post intravenous (IV) injection.

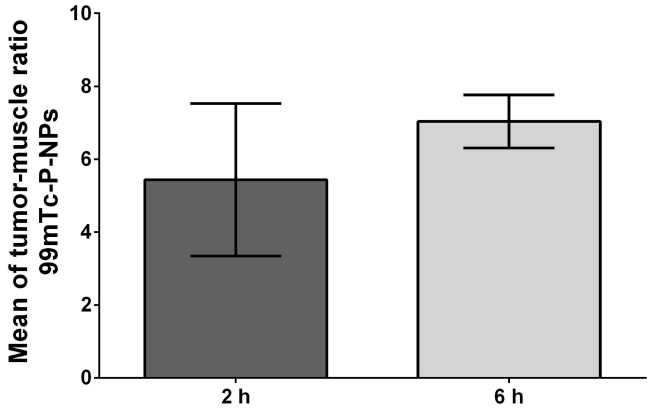


**Figure 12** Mean of tumor–muscle ratio uptake in 4T1 tumor-bearing Balb/C mice ($n$ = 3) evaluated by SPECT at 2 and 6 h post intravenous (IV) injection of $^{99m}$Tc-P-NPs.

and high staining for papain in the tumor slice, indicating targeted affinity to tumoral cells, reinforcing that P-NPs were selectively absorbed in the tumor region in both animal models evaluated in this study (4T1 and MMTV-PyMT).

## Discussion

The present study delves into the innovative application of P-NPs as a potential cancer imaging agent, combining the unique properties of papain with the versatility of nano and radiation technology to crosslink protein nanoparticles by gamma irradiation. The focus on plant proteases, particularly papain, for designing protein nanoparticles is a strategic move owing to its advantageous physicochemical and biological properties besides its proven therapeutic benefits, including anticancer, antibacterial, and antioxidant capabilities.

The synthesized P-NPs, as detailed in the results section, exhibit promising characteristics. Their small size and spherical nature make them potential candidates for effective drug delivery systems. The negative zeta adds a layer of stability, crucial for their intended biological applications. The mechanism of nanoparticle formation through ionizing radiation-induced crosslinking occurs primarily via free radicals generated from the radiolysis of water in the protein solution. The exposure of proteins to these reactive species causes conformational changes, leading to covalent bonds, such as bityrosine, which are considered one of the main bonds involved in protein crosslinking.[9,48] This method offers

significant advantages over conventional methods, allowing for simultaneous sterilization of the vial contents during the synthesis reaction. Furthermore, the absence of cross-linking agents ensures low residual toxicity, reducing the need for additional purification steps to remove remaining monomers.[49]

Concerning biocompatibility, the in vitro cytotoxicity assessment of native papain and P-NPs on non-tumoral cells (HUVEC) provided valuable insights into their safety profile. The minimal cytotoxicity observed in most conditions, especially in the case of P-NPs, lays a solid foundation for further exploration of their biomedical applications. Additionally, papain concentrations of up to 100 $\mu g.mL^{-1}$ had no significant effects on the growth of HUVEC cells. Still, the inactivation of Vascular Endothelial Growth Factors (VEGF) demonstrated a substantial antiangiogenic effect of papain, indicating an exceptional potential for application as a preventative and therapeutic agent in diseases involving angiogenic processes.[17]

The successful radiolabeling of P-NPs with technetium-99m opens exciting avenues for nuclear imaging. To validate the robustness of the developed system, detailed standardization of radiolabeling parameters and subsequent stability analysis were conducted. Several studies on protein radiolabeling have been published, featuring diverse methods such as direct and indirect radiolabeling (bifunctional chelator) protocols. For radiolabeling P-NPs, the direct pathway was chosen, utilizing a tin chloride solution ($SnCl_2$) to reduce the oxidation state of $^{99m}Tc$ atoms. This reduction process facilitates the formation of radiometal complexes with reactive groups present on the protein surface, including carboxyl (-COOH), hydroxyls (-OH), amino ($-NH_2$), and thiols (-SH) groups. This method, owing to its ease, availability, and reproducibility, is commonly employed in preparing various radiopharmaceuticals labeled with $^{99m}Tc$. Eluates with high specific activity were crucial for achieving high yield and radiochemical purity. This was a Radiopharmaceuticals accomplished by utilizing elution from the $^{99}Mo/^{99m}Tc$ generator, with a preceding 24-hour period to ensure optimal conditions. One notable advantage of this strategy is the reduction of the long half-life isotope $^{99}Tc$, formed during $^{99}Mo$ and $^{99m}Tc$ decays. This is important as the presence of $^{99}Tc$ can compete and compromise the radiolabeling yield. The radiolabeling of papain nanoparticles with $^{99m}Tc$ demonstrated a radiochemical purity exceeding 90%, aligning with the standards set by the US Pharmacopeia (USP) and European Pharmacopoeia (Ph. Eur). for most radiopharmaceuticals.[50]

Beyond the in vitro biocompatibility success and the observed stability of the $^{99m}Tc$-P-NPs complex in histidine solution and human serum, it holds promise, paving the way for potential in vivo applications. Before delving into in vivo studies, a critical assessment of the in vitro stability of the $^{99m}Tc$-P-NPs complex under conditions mimicking the biological milieu was imperative.[42] This involved subjecting the complex to a histidine challenge, leveraging the endogenous amino acid known for its high concentrations in vivo and its propensity to induce instability in $^{99m}Tc$ radiolabeled compounds due to transchelation. The results, revealing the stability of $^{99m}Tc$-P-NPs for up to 6 h post-radiolabeling, mark a significant stride in understanding the potential of this radiolabeling approach for future applications.

In the biological evaluation section, the in vitro cell binding studies underscore the tumor-targeting prowess of $^{99m}Tc$-P-NPs, with time-dependent cellular uptake and internalization in breast cancer cell lines revealing their potential as effective imaging agents. Subsequent in vivo biodistribution studies in healthy and tumor-bearing mice further substantiate the translational potential of $^{99m}Tc$-P-NPs. The observed clearance patterns, notably the predominant role of the renal-urinary system, align with the desirable attributes of an effective imaging agent once renal excretion is the primary elimination route attributed to particle size. The kidneys, efficient in eliminating particles with a diameter ≤10 nm, play a significant role, while the liver eliminates larger particles. Uptakes in organs with a mononuclear phagocytic system (MPS), such as the liver and spleen, align with established literature acknowledging MPS macrophages' rapid opsonization and removal of nanoparticles from circulation.[51] Noteworthy is the low uptake observed in other organs studied, including the stomach and thyroid, throughout the experiment. This data assumes significance as it indicates that the $^{99m}TcO_4^-$ concentration, a radiochemical impurity formed during the radiolabeling process, and free technetium remain within recommended limits, given their preferential uptake in these organs.[52]

Regarding tumor uptake, the radioactivity detected in normal tissue, specifically muscle, is notably lower compared to tumors, as illustrated in Figure 8 and Table S1. The mean tumor/muscle ratio derived from these findings suggests a pronounced affinity for tumor tissue, demonstrating promising future applications of $^{99m}Tc$-P-NPs for molecular imaging of tumors. This observation is further supported by the SPECT/CT images, which consistently depict a stronger affinity for tumor tissue than normal muscles across all examined time intervals.

Our investigation underscores the pivotal role of Alpha-2-macroglobulin and Alpha-1 antitrypsin in binding, targeting, and transporting papain to tumor tissue—all of which influence the delicate balance between proteinase and antiproteinase.[53] It may be noted that the P-NP tumor uptake, as shown in our investigation, is presumably a result of passive targeting facilitated by solid tumors through enhanced permeation and retention (EPR) effects. This phenomenon results from blood vessels leading to tumor membranes due to their rapid and defective production during tumor angiogenesis, resulting in fenestrations and low endothelial cell adhesion.[54]

Beyond the EPR effect, another hypothesis which has been validated in the current investigation is that the papain proteolytic activity contributes to the degradation of the extracellular matrix (ECM), thereby facilitating the diffusion of nanoparticles into the tumor interstitium. The choice of papain as an enzymatic nanocarrier is motivated by the potential to modulate the tumor microenvironment, overcome penetration obstacles, and enhance administration efficiency due to the ECM's high susceptibility to protease activity.[54–57]

The ECM, an intrinsic biological barrier surrounding the tumor parenchyma, comprises proteoglycans, hyaluronic acid, collagen, elastin, laminin, and other structural proteins. Notably, it hinders the diffusion of drugs, therapeutic macromolecules, and nanocarriers in cells distant from blood vessels.[58–60] Leveraging ECM degradation for tumor microenvironment modulation has been acknowledged in the literature as an effective strategy for increasing nanoparticle uptake. This multifaceted approach, combining passive targeting through the EPR effect and active modulation of the ECM, holds promise for optimizing the delivery of therapeutic agents to tumor tissues.

As discussed above, our results put the overall field of nanoparticulate-based molecular imaging and therapy agents into perspective. The tremendous clinical implications of nanosized molecular imaging, therapeutic and theranostic agents encompass various aspects of oncology into neuro-oncology—all aimed at enhancing contrast agents and radiotracers for the accurate delineation of clinical outcomes in diagnostic radiology and nuclear medicine.[61,62]

## Conclusion

The aforementioned results of our investigation, for the first time, has demonstrated unequivocally that papain nanoparticles, produced through innovative green nanotechnology, offer an ideal chemical backbone of optimal ligating characteristics capable of forming in vivo stable bonds with Tc-99m. Detailed in vitro tumor cell binding and internalization investigations showed tumor-targeting prowess of $^{99m}$Tc-P-NPs for potential molecular imaging of breast and other tumors through SPECT/CT imaging.

Complete biodistribution assays, confirmed by STECT/CT imaging, demonstrated a higher affinity of the $^{99m}$Tc-P-NPs nanoparticles to breast tumor tissues as compared to normal tissues at all time points. Therefore, the present study has opened new opportunities towards the application of papain nanoparticles as carriers of diagnostic and therapeutic radionuclides to deliver diagnostic/therapeutic payloads site-specifically to tumor sites for the development of new generation of nanoradiopharmaceuticals. However, the limitations of this study, such as the need for further in vivo validation and potential long-term toxicity, should be addressed in future research.

## Acknowledgments

Conselho Nacional de Desenvolvimento Científico e Tecnológico (CNPq) and International Atomic Energy Agency (IAEA) Coordinated Research Project: Nanosized Delivery Systems for Radiopharmaceuticals (CRP code: F22064)

## Disclosure

The authors declare no conflict of interest.

## References

1. Madamsetty VS, Mukherjee A, Mukherjee S. Recent trends of the bio-inspired nanoparticles in cancer theranostics. *Front Pharmacol*. 2019;10:1264. doi:10.3389/FPHAR.2019.01264/BIBTEX
2. Jin C, Wang K, Oppong-Gyebi A, Hu J. Application of nanotechnology in cancer diagnosis and therapy - a mini-review. *Int J Med Sci*. 2020;17(18):2964. doi:10.7150/IJMS.49801
3. Freitas LF, Ferreira AH, Thipe VC, et al. The state of the art of theranostic nanomaterials for lung, breast, and prostate cancers. *Nanomaterials*. 2021;11(10):2579. doi:10.3390/NANO11102579

4. Khoobchandani M, Katti KK, Karikachery AR, et al. New approaches in breast cancer therapy through green nanotechnology and nano-ayurvedic medicine - pre-clinical and pilot human clinical investigations. *Int J Nanomed*. 2020;15:181–197. doi:10.2147/IJN.S219042
5. Thakur V, Kutty RV. Recent advances in nanotheranostics for triple negative breast cancer treatment. *J Exp Clin Cancer Res*. 2019;38(1):1–22. doi:10.1186/S13046-019-1443-1
6. Hou K, Ning Z, Chen H, Wu Y. Nanomaterial technology and triple negative breast cancer. *Front Oncol*. 2021;11. doi:10.3389/FONC.2021.828810
7. Silva-López RE, Gonçalves RN. Therapeutic proteases from plants: biopharmaceuticals with multiple applications. *J Appl Biotechnol Bioengin*. 2019;6(Issue 2):101–109. doi:10.15406/JABB.2019.06.00180
8. de Lima CSA, Rial-Hermida MI, de Freitas LF, et al. Mucoadhesive gellan gum-based and carboxymethyl cellulose -based hydrogels containing gemcitabine and papain for bladder cancer treatment. *Int J Biol Macromol*. 2023;242(Pt 3):124957. doi:10.1016/J.IJBIOMAC.2023.124957
9. Fazolin GN, Varca GHC, Kadlubowski S, Sowinski S, Lugão AB. The effects of radiation and experimental conditions over papain nanoparticle formation: towards a new generation synthesis. *Radiat Phys Chem*. 2020;169:107984. doi:10.1016/J.RADPHYSCHEM.2018.08.033
10. de Lima CSA, Varca JP, Nogueira KM, et al. Semi-solid pharmaceutical formulations for the delivery of papain nanoparticles. *Pharmaceutics*. 2020;12(12):1–12. doi:10.3390/PHARMACEUTICS12121170
11. Budama-Kilinc Y, Cakir-Koc R, Kecel-Gunduz S, et al. Papain Loaded Poly(ε-Caprolactone) nanoparticles: in-silico and in-vitro studies. *J Fluoresc*. 2018;28(5):1127–1142. doi:10.1007/S10895-018-2276-6
12. Zhang M, Wei Z, Chang S, Teng M, Gong W. Crystal structure of a papain-fold protein without the catalytic residue: a novel member in the cysteine proteinase family. *J Mol Biol*. 2006;358(1):97–105. doi:10.1016/J.JMB.2006.01.065
13. Leite AP, de OBGRB, Soares MF, Barrocas DLR. Use and effectiveness of papain in the wound healing process: a systematic review. *Rev Gaucha Enferm*. 2012;33(3):198–207. doi:10.1590/S1983-14472012000300026
14. Gremmler L, Kutschan S, Dörfler J, Büntzel J, Büntzel J, Hübner J. Proteolytic enzyme therapy in complementary oncology: a systematic review. *Anticancer Res*. 2021;41(7):3213–3232. doi:10.21873/ANTICANRES.15108
15. Beuth J, Ost B, Pakdaman A, et al. Impact of complementary oral enzyme application on the postoperative treatment results of breast cancer patients--results of an epidemiological multicentre retrolective cohort study. *Cancer Chemother Pharmacol*. 2001;(47 Suppl):S45–54. doi:10.1007/s002800170009
16. Nguyen TTT, Shaw PN, Parat MO, Hewavitharana AK. Anticancer activity of Carica papaya: a review. *Mol Nutr Food Res*. 2013;57(1):153–164. doi:10.1002/MNFR.201200388
17. Mohr T, Desser L, Obikeze K. Plant proteolytic enzyme papain abrogates angiogenic activation of human umbilical vein endothelial cells (HUVEC) in vitro. *BMC Complement Altern Med*. 2013;13. doi:10.1186/1472-6882-13-231
18. Wald M, Olejár T, Šebková V, Zadinová M, Boubelík M, Poučková P. Mixture of trypsin, chymotrypsin and papain reduces formation of metastases and extends survival time of C57Bl6 mice with syngeneic melanoma B16. *Cancer Chemother Pharmacol*. 2001;47(7):S16–S22. doi:10.1007/S002800170004
19. Müller A, Barat S, Chen X, et al. Comparative study of antitumor effects of bromelain and papain in human cholangiocarcinoma cell lines. *Int J Oncol*. 2016;48(5):2025–2034. doi:10.3892/IJO.2016.3411
20. Otsuki N, Dang NH, Kumagai E, Kondo A, Iwata S, Morimoto C. Aqueous extract of Carica papaya leaves exhibits anti-tumor activity and immunomodulatory effects. *J Ethnopharmacol*. 2010;127(3):760–767. doi:10.1016/J.JEP.2009.11.024
21. Wald M, Závadová E, Poučková P, Zadinová M, Boubelik M. Polyenzyme preparation Wobe-Mugos inhibits growth of solid tumors and development of experimental metastases in mice. *Life Sci*. 1998;62(3):PL43–8.
22. Sakalová A, Bock PR, Dedík L, et al. Retrolective cohort study of an additive therapy with an oral enzyme preparation in patients with multiple myeloma. *Cancer Chemother Pharmacol*. 2001:47(7):S38–S44. doi:10.1007/S002800170008
23. Chandran SP, Nachimuthu K. Immunostimulatory potential of papain encapsulated solid lipid nanoparticles. *J Appl Pharm Sci*. 2018;8(07):37–042. doi:10.7324/JAPS.2018.8707
24. Wald M. Exogenous proteases confer a significant chemopreventive effect in experimental tumor models. *Integr Cancer Ther*. 2008;7(4):295–310. doi:10.1177/1534735408327036
25. Beuth J. Proteolytic enzyme therapy in evidence-based complementary oncology: fact or fiction? *Integr Cancer Ther*. 2008;7(4):311–316. doi:10.1177/1534735408327251
26. Parodi A, Haddix SG, Taghipour N, et al. Bromelain surface modification increases the diffusion of silica nanoparticles in the tumor extracellular matrix. *ACS Nano*. 2014;8(10):9874–9883. doi:10.1021/NN502807N/SUPPL_FILE/NN502807N_SI_004.PDF
27. Shukla R, Chanda N, Zambre A, et al. Laminin receptor specific therapeutic gold nanoparticles (198AuNP-EGCg) show efficacy in treating prostate cancer. *Proc Natl Acad Sci U S A*. 2012;109(31):12426–12431. doi:10.1073/pnas.1121174109
28. Cutler C, Kan P, Chanda N, et al. Preparation and use of 198Au/199Au for potential applications in cancer therapy and imaging. *Trans Am Nucl Soc*. 2010;103:1123–1124.
29. Al-Yasiri AY, Khoobchandani M, Cutler CS, et al. Mangiferin functionalized radioactive gold nanoparticles (MGF-198AuNPs) in prostate tumor therapy: green nanotechnology for production,: in vivo tumor retention and evaluation of therapeutic efficacy. *Dalton Trans*. 2017;46 (42):14561–14571. doi:10.1039/c7dt00383h
30. Chanda N, Kan P, Watkinson LD, et al. Radioactive gold nanoparticles in cancer therapy: therapeutic efficacy studies of GA- 198 AuNP nanoconstruct in prostate tumor – bearing mice. *Nanomedicine*. 2010;6(2):201–209. doi:10.1016/j.nano.2009.11.001
31. Chanda N, Kattumuri V, Shukla R, et al. Bombesin functionalized gold nanoparticles show in vitro and in vivo cancer receptor specificity. *Proc Natl Acad Sci*. 2010;107(19):8760–8765. doi:10.1073/pnas.1002143107
32. Al-Yasiri AY, White NE, Katti KV, Loyalka SK. Estimation of tumor and local tissue dose in gold nanoparticles radiotherapy for prostate cancer. *Rep Pract Oncol Radiother*. 2019;24(3):288–293. doi:10.1016/j.rpor.2019.02.006
33. Katti KV. Renaissance of nuclear medicine through green nanotechnology: functionalized radioactive gold nanoparticles in cancer therapy—my journey from chemistry to saving human lives. *J Radioanal Nucl Chem*. 2016;309(1):5–14. doi:10.1007/s10967-016-4888-0
34. Sakr TM, Morsy SAG, Mahmoud NA, et al. *Preparation, Characterization, Cytotoxicity and Biological Evaluation of 99mtc-Doxorubicin-Epigallocatechingallate Functionalized Gold Nanoparticles as a New Generation of Theranostic Radiopharmaceutical*. Preprints; 2018. doi:10.20944/preprints201808.0331.v1
35. Khoobchandani M, Khan A, Katti KVKK, et al. Green nanotechnology of MGF-AuNPs for immunomodulatory intervention in prostate cancer therapy. *Sci Rep*. 2021;11(1):16797. doi:10.1038/s41598-021-96224-8

36. Khoobchandani M, Al-Yasiri AY, Katti YKK, et al. Prostate tumor therapy advances in nuclear medicine: green nanotechnology toward the design of tumor specific radioactive gold nanoparticles. *J Radioanal Nucl Chem*. 2018;318(3):1737–1747. doi:10.1007/s10967-018-6320-4
37. Thipe VC, Karikachery AR, Çakılkaya P, et al. Green nanotechnology—An innovative pathway towards biocompatible and medically relevant gold nanoparticles. *J Drug Deliv Sci Technol*. 2022;70(March). doi:10.1016/j.jddst.2022.103256
38. Katti K, Khan A, Mutalik V. Ayurvedic encapsulated gold nanoparticles, fabrication methods and cancer therapeutic methods. *United States Patent US*. 2021;2021:1–60.
39. Varca GHC, Queiroz RG, Lugão AB. Irradiation as an alternative route for protein crosslinking: cosolvent free BSA nanoparticles. *Radiat Phys Chem*. 2016;124:111–115. doi:10.1016/J.RADPHYSCHEM.2016.01.021
40. De Silva L, Fu JY, Htar TT, et al. Characterization, optimization, and in vitro evaluation of Technetium-99m-labeled niosomes. *Int J Nanomed*. 2019;14:1101–1117. doi:10.2147/IJN.S184912
41. Gundogdu E, Demir ES, Özgenç E, Yeğen G, Aksu B. Applying Quality by Design Principles in the Development and Preparation of a New Radiopharmaceutical: technetium-99m-Imatinib Mesylate. *ACS Omega*. 2020;5(10):5297–5305. doi:10.1021/ACSOMEGA.9B04327
42. Gaonkar RH, Ganguly S, Dewanjee S, et al. Garcinol loaded vitamin E TPGS emulsified PLGA nanoparticles: preparation, physicochemical characterization, in vitro and in vivo studies. *Sci Rep*. 2017;7(1):1–14. doi:10.1038/s41598-017-00696-6
43. Gaonkar RH, Ganguly S, Baishya R, et al. Exploring the Potential of 99mTc(CO)3-labeled triazolyl peptides for tumor diagnosis. *Cancer Biother. Radiopharm*. 2016;31(3):110–117. doi:10.1089/CBR.2015.1915
44. Wang R, Wang X, Jia X, Wang H, Li W, Li J. Impacts of particle size on the cytotoxicity, cellular internalization, pharmacokinetics and biodistribution of betulinic acid nanosuspensions in combined chemotherapy. *Int J Pharm*. 2020;588:119799. doi:10.1016/J.IJPHARM.2020.119799
45. Biagiotti G, Pisaneschi F, Gammon ST, et al. Multiwalled carbon nanotubes for combination therapy: a biodistribution and efficacy pilot study. *J Mater Chem B*. 2019;7(16):2678–2687. doi:10.1039/C8TB03299H
46. Schrörs B, Boegel S, Albrecht C, et al. Multi-omics characterization of the 4T1 murine mammary gland tumor model. *Front Oncol*. 2020;10:1195. doi:10.3389/FONC.2020.01195/BIBTEX
47. Christenson JL, Butterfield KT, Spoelstra NS, et al. MMTV-PyMT and derived Met-1 mouse mammary tumor cells as models for studying the role of the androgen receptor in triple-negative breast cancer progression. *Horm Cancer*. 2017;8(2):69. doi:10.1007/S12672-017-0285-6
48. Ferreira AH, Lima CSA, Cunha da Cruz CP, et al. Experimental design of size variation in albumin nanoparticles synthesized by electron beam. *Radiat Phys Chem*. 2024;223:111974. doi:10.1016/J.RADPHYSCHEM.2024.111974
49. Queiroz RG, Varca GHC, Kadlubowski S, Ulanski P, Lugão AB. Radiation-synthesized protein-based drug carriers: size-controlled BSA nanoparticles. *Int J Biol Macromol*. 2016;85:82–91. doi:10.1016/J.IJBIOMAC.2015.12.074
50. Hubers D, Scott PJH. *Chapter 4:Design and Synthesis of Radiopharmaceuticals for SPECT Imaging*. In: *2011-2015 Analytical Chemistry Subject Collection*. Royal Society of Chemistry; 2011:144–172. doi:10.1039/9781849732918-00144
51. Song G, Petschauer J, Madden A, Zamboni W. Nanoparticles and the mononuclear phagocyte system: pharmacokinetics and applications for inflammatory diseases. *Curr Rheumatol Rev*. 2014;10(1):22–34. doi:10.2174/1573403X10666140914160554
52. Griffin N, Grant LA. Endocrine system. *Graing Allison's Diagnost Radiol Essent*. 2013;856–871. doi:10.1016/B978-0-7020-3448-0.00058-X
53. Li T, Yan G, Bai Y, et al. Papain bioinspired gold nanoparticles augmented the anticancer potency of 5-FU against lung cancer. *J Exp Nanosci*. 2020;15(1):109–128. doi:10.1080/17458080.2020.1746767
54. Jain RK, Stylianopoulos T. Delivering nanomedicine to solid tumors. *Nat Rev Clin Oncol*. 2010;7(11):653–664. doi:10.1038/nrclinonc.2010.139
55. Eikenes L, Tari M, Tufto I, Bruland S, De Lange Davies C. Hyaluronidase induces a transcapillary pressure gradient and improves the distribution and uptake of liposomal doxorubicin (CaelyxTM) in human osteosarcoma xenografts. *Br J Cancer*. 2005;93(1):81–88. doi:10.1038/sj.bjc.6602626
56. Ganesh S, Gonzalez-Edick M, Gibbons D, Van Roey M, Jooss K. Intratumoral coadministration of hyaluronidase enzyme and oncolytic adenoviruses enhances virus potency in metastatic tumor models. *Clin Cancer Res*. 2008;14(12):3933–3941. doi:10.1158/1078-0432.CCR-07-4732
57. Gullotti E, Yeo Y. Extracellularly activated nanocarriers: a new paradigm of tumor targeted drug delivery. *Mol Pharm*. 2009;6(4):1041–1051. doi:10.1021/MP900090Z
58. Engin AB, Nikitovic D, Neagu M, et al. Mechanistic understanding of nanoparticles' interactions with extracellular matrix: the cell and immune system. *Particle and Fibre Toxicology*. 2017;14(1):1–16. doi:10.1186/S12989-017-0199-Z
59. Nallanthighal S, Heiserman JP, Cheon DJ. The role of the extracellular matrix in cancer stemness. *Front Cell Dev Biol*. 2019;7:86. doi:10.3389/FCELL.2019.00086/BIBTEX
60. Järveläinen H, Sainio A, Koulu M, Wight TN, Penttinen R. Extracellular matrix molecules: potential targets in pharmacotherapy. *Pharmacol Rev*. 2009;61(2):198. doi:10.1124/PR.109.001289
61. Ganau M. Tackling gliomas with nanoformulated antineoplastic drugs: suitability of hyaluronic acid nanoparticles. *Clin Transl Oncol*. 2014;16(2):220–223. doi:10.1007/S12094-013-1114-1
62. Ganau M, Syrmos NC, D'Arco F, et al. Enhancing contrast agents and radiotracers performance through hyaluronic acid-coating in neuroradiology and nuclear medicine. *Hell J Nucl Med*. 2017;20(2):166–168. doi:10.1967/S002449910558